Journal of Oceanography
Vol. 51, pp. 571 to 584. 1995

An Application of a Two-Layer Model to Wind Driven Sub-Tidal Currents in Puget Sound

H. MATSUURA

School of Oceanography, University of Washington, Seattle, WA 98195, U.S.A.

(Received 5 December 1994; in revised form 27 March 1995; accepted 29 March 1995)

A two layer model of an infinitely long channel, with one end closed, is applied to study the sub-tidal response to wind forcing of Puget Sound. The model uses a linear friction parameterization. Data show that the acceleration of current near the surface responds to the wind event almost instantaneously, however, acceleration tends to start decreasing at later times and eventually changes sign even though the wind blows in one direction throughout. Analysis of the model results show that when the forcing frequency is high, the phase lag between forcing and friction causes this phenomena, and as forcing frequency increases, phase lag between forcing and friction approaches $\pi/2$. When the forcing frequency is low, phase lag between forcing and friction decreases almost linearly with forcing frequency and at extremely low frequency, they almost balance each other. Analysis of the model results show also that the amplitude of baroclinic pressure gradient increases rapidly as forcing frequency decreases and when the forcing frequency is low, the baroclinic pressure gradient becomes important. Effects of baroclinic pressure gradient propagate as a wave from the boundaries and it takes about one day to take effect at the point where the observations were made.

1. Introduction

The typical fjord circulation, as described in many texts, is based on the two-layer circulation. The surface water flows out from a fjord due to run-off. As the surface water flows toward the mouth, the volume of outflow increases due to the increase of salinity by mixing and entrainment. To compensate for this increased volume, there is a mid-depth inflow of water. However, winds may significantly alter this picture. Hansen and Rattray (1965) studied steady state fjord circulation using a similarity method. They showed that the depth of the maximum return flow decreases as down-fjord wind stress increases, while the amplitude of the return flow increases. Farmer (Farmer, 1976; Farmer and Osborn, 1976) studied the wind effects in Alberni Inlet, B.C., Canada, a highly stratified fjord with a thin surface layer. He used a two layer model and compared it with actual data for the displacement of the pycnocline. Their model results (Figs. 11 and 12, Farmer, 1976) appear to match the observations well. Buckley and Pond (1976) found that with continuous up-fjord wind, the surface current was reversed initially, but it reversed again after a certain time as if the wind stopped (Fig. 6, Buckley and Pond). Their explanation was that at the second reversing, a balance between wind stress and pressure gradient was achieved. Svendsen and Thompson (1978) made observations of currents in a Norwegian fjord not only at the surface but also at depths greater than the depth of the pycnocline. They showed that the first response to wind occurs at the surface but the second response was at a

*Current Address; 2-17-4-301, Zoushigaya, Teshima, Tokyo, Japan.

somewhat greater depth (60 m) below the pycnocline (10 m), and the response gradually propagated upward through the water column (Fig. 10, Svendsen and Thompson). More recently Tee (1989) showed meteorological effects in the St. Lawrence estuary at different time scales ranging from 11 to 40–50 day periods. He showed that at the fortnight period band, wind makes a considerable contribution to the total variance at depths greater than 20 m.

Puget Sound is a fjord type estuary which is connected to the North Pacific through the Strait of Juan de Fuca. The portion studied here is the main basin south of Admiralty Inlet and north

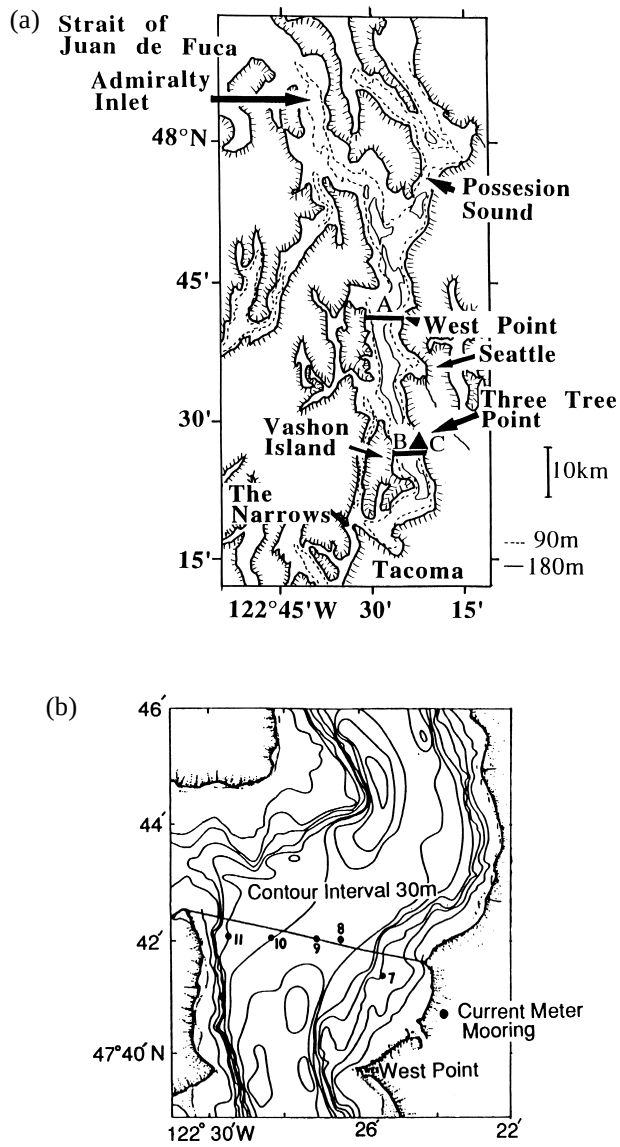

Fig. 1. (a) A map of Puget Sound. The contours of the bottom at 90 m and 180 m are shown in the figure. The solid triangle (C) is the location of the weather station. The solid line A shows the location of the 1985 observation site. (b) The locations of moorings (solid dots) of 1985 observation off West Point shown as the line A in Fig. 1(a). The position of M6 is too close to M9 and not shown in this figure.

of the Narrows, near Tacoma (Fig. 1(a)). The bathymetry of the main basin is fairly flat, the bottom depth is about 200 m, and it is bounded by sill zones both seaward and landward. The seaward sill zone is located in Admiralty Inlet. This sill zone is relatively long and consists of two sills, 65 m and 105 m deep. The landward sill is located in the Narrows with a depth of 45 m.

The general sub-tidal circulation pattern in the main basin follows the classical fjord type. However, several authors (Cannon and Laird, 1978; Cannon, 1983; Bretschneider *et al*., 1985) noted that wind has significant effects on sub-tidal circulation. Among them, Bretschneider *et al*. (1985) used empirical orthogonal function (EOF) analysis applied to the along channel currents near Three Tree Point (Line B, Fig. 1(a)). They found that the most dominant EOF (mode 1) was dominated by wind effects and showed strong influence at the surface, and weak but statistically significant counter-influence at mid-depths on axial currents near Three Tree Point. The second EOF mode was associated with bottom water intrusions, and the third was related to the circulation around Vashon Island. Although they pointed out that EOF mode 1 was wind caused, further details were omitted. This study attempts to expand on their results.

2. Observations

In this section, we briefly summarize observed wind effects on the sub-tidal currents. More detailed descriptions may be found in Matsuura (1992) and the author is currently preparing a paper which describes the detail of observations.

The data used in this paper were collected in 1985 from mid April to mid June at six moorings off West Point (Line A, Fig. 1(a); Fig. 1(b), The position of M6 is very close to the position of M9 and not noted in this figure). Among these six moorings, near surface currents were measured at M6 and M10. The vertical positions of current meters, excluding those which failed, are shown in Table 1. Wind was measured at Three Tree Point (position C in Fig. 1(a)).

The correlation analysis between axial wind speed and axial currents shows high positive correlation near the surface (0.80 at 4 m at M6) and weak but statistically significant negative correlation at mid-depth (–0.36 at 104 m at M9). It is quite often seen that acceleration of the flow near the surface reaches a maximum and starts decreasing before the wind reaches its maximum. It then changes sign (against the wind, decelerates) even though the wind still blows in the same direction. This phenomena will be explored in the subsequent section (Fig. 6). The result of EOF analysis applied to the axial currents shows that the coherence between EOF mode 1 and axial

Table 1. The depths of current meters. The unit of depths is one m.

M7	M8	M6/9	M10	M11
—	—	4	5	—
—	—	10	—	—
26	22	19	22	19
47	—	40	42	41
76	69	70	73	71
	106	104	111	—
	152	—	153	158
	185	178	179	
		195		

wind speed is higher than 0.8 in almost the entire frequency range, and it suggests that this component is primarily caused by wind. EOF mode 1 contains 69% of total variance. The distribution of eigenvectors shows maxima at the surface and at about 100 m, approximately at the center of channel, but of opposite sign. Prior to this EOF analysis, a band-pass filter (0.1 cpd to 0.7 cpd) is applied to eliminate both high frequency components such as diurnal tides and low frequency components such as the fortnight tide.

3. Two-Layer Model

In this section, a two-layer model is introduced. The model has the same boundary conditions as Farmer (1976). Later in this section, the comparisons between the observations and the model are made and the effects of forcing frequency are discussed.

3.1 Solutions

Farmer (1976, hereafter FA) developed a two-layer model to investigate wind effects on the surface-layer thickness. He used a linear friction applied to transport, which represents side, bottom and interfacial stress. The channel was infinitely long with one end. Uniform wind stress was applied from the head at $x = 0$ to the mouth at $x = d$. The bottom was flat, and no sill existed at $x = d$. Figure 2 shows the configuration of his model. The equations of motion of the baroclinic mode are, following FA,

$$\frac{\partial u}{\partial t} = C^2 \frac{\partial \eta}{\partial x} + Tw - ru \qquad \text{for } 0 \le x < d \tag{1}$$

$$\frac{\partial u}{\partial t} = C^2 \frac{\partial \eta}{\partial x} - ru \qquad \text{for } d \le x \tag{2}$$

where u is the transport and defined by $u \equiv (h_2 u_1 - h_1 u_2)/h$, h is the total depth, h_1 is the upper layer thickness, h_2 is the lower layer thickness at rest, C is the phase speed defined by $C = [gh_1h_2(\rho_2 - \rho_1)/(\rho_2 h)]^{1/2}$, ρ_1 is the density in the upper layer, ρ_2 is the density in the lower layer, η is the perturbation of the surface layer thickness from the rest state defined by $\eta \equiv \eta_2 - \eta_1$, r is the friction coefficient, Tw is the forcing term and defined as $Tw \equiv Wh_2/h$, and W is the wind stress and is a function of time only, respectively. The boundary conditions are $u = 0$ at $x = 0$ and

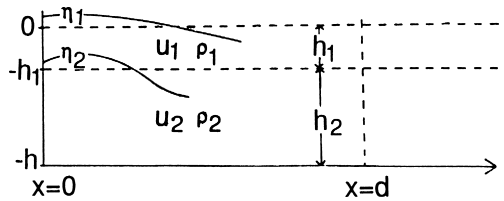

Fig. 2. The configuration of the Farmer's model. The channel is infinitely long but has one end at $x = 0$. The position, $x = d$, represents the position of the mouth and wind is applied only at $0 \le x < d$. η_1, u_1, ρ_1, η_2, u_2 and ρ_2 are the surface perturbation, the transport and the density in the upper layer, the interface perturbation, the transport and density in the lower layer, respectively. T he surface layer thickness at rest is h_1 and the lower layer thickness at rest is $h - h_1$.

$x = \infty$. Wind stress, W, is applied only between $x = 0$ and $x = d$, the interior to the fjord. The matching conditions are that both u and η are continuous at $x = d$.

Farmer solved this problem as an initial/boundary value problem and a boundary value problem. His solution of the initial/boundary value problem for the surface layer thickness was

$$\eta = \frac{1}{C}\int_0^t \left[Tw(t-\tau)e^{-r\tau/2} \left\{ I_0\left[\frac{r}{2}\left(\tau^2 - \frac{x^2}{C^2}\right)^{1/2}\right] H\left[\tau - \frac{x}{C}\right] \right.\right.$$
$$- \frac{1}{2} I_0\left[\frac{r}{2}\left(\tau^2 - \frac{(x+d)^2}{C^2}\right)^{1/2}\right] H\left[\tau - \frac{x+d}{C}\right]$$
$$\left.\left. - \frac{1}{2} I_0\left[\frac{r}{2}\left(\tau^2 - \frac{(d-x)^2}{C^2}\right)^{1/2}\right] H\left[\tau - \frac{d-x}{C}\right] \right\} \right] d\tau \quad \text{for } 0 \le x < d \tag{3}$$

where I_0 is the modified Bessel function of order of 0 and H is the Heaviside function.

Velocity is the measured parameter in our case and therefore solution for the transport is necessary. Transport is obtained from Eq. (1),

$$u = e^{-rt}\int_0^t \left(C^2 \frac{\partial \eta(x,\tau)}{\partial x} + Tw(\tau) \right) e^{r\tau} d\tau \tag{4}$$

$\partial\eta/\partial x$ is evaluated from Farmer's solution, Eq. (3),

$$\frac{\partial \eta}{\partial x} = \frac{1}{C}\int_0^t \left[Tw(t-\tau)e^{-r\tau/2} \left\{ -\frac{rx}{2C^2}\left(\tau^2 - \frac{x^2}{C^2}\right)^{-1/2} I_1\left[\frac{r}{2}\left(\tau^2 - \frac{x^2}{C^2}\right)^{1/2}\right] H\left(\tau - \frac{x}{C}\right) \right.\right.$$
$$+ \frac{r(x+d)}{4C^2}\left(\tau^2 - \frac{(x+d)^2}{C^2}\right)^{-1/2} I_1\left[\frac{r}{2}\left(\tau^2 - \frac{(x+d)^2}{C^2}\right)^{1/2}\right] H\left(\tau - \frac{x+d}{C}\right)$$
$$\left.\left. - \frac{r(d-x)}{4C^2}\left(\tau^2 - \frac{(d-x)^2}{C^2}\right)^{-1/2} I_1\left[\frac{r}{2}\left(\tau^2 - \frac{(d-x)^2}{C^2}\right)^{1/2}\right] H\left(\tau - \frac{d-x}{C}\right) \right\} \right] d\tau$$
$$+ \frac{1}{C^2}\left\{ -Tw\left(t - \frac{x}{C}\right)e^{-\frac{rx}{2C}} + \frac{1}{2}Tw\left(t - \frac{x+d}{C}\right)e^{-\frac{r(x+d)}{2C}} - \frac{1}{2}Tw\left(t - \frac{d-x}{C}\right)e^{-\frac{r(d-x)}{2C}} \right\} \tag{5}$$

where I_1 is the modified Bessel function of the first order. Note that $\partial\eta/\partial x$ is zero until the wave fronts reach the point x either from the mouth or the head.

If $r = 0$ (no friction), all the terms inside of the integrand in Eq. (5) are zero. In this case, if

constant forcing is suddenly turned on at $t = 0$ as $Tw = TH(t)$, where T is a constant and H is the Heaviside function, then

$$u = T\int_0^t \left\{ -H\left(\tau - \frac{x}{C}\right) + \frac{1}{2}H\left(\tau - \frac{x+d}{C}\right) - \frac{1}{2}H\left(\tau - \frac{d-x}{C}\right) + H(\tau) \right\} d\tau. \tag{6}$$

The first term represents the response propagated from the head, the second term the response propagated from the mouth and then reflected at the head, and the third term the response propagated from the mouth. The last term is locally driven and comes from Tw in Eq. (4). Between $t = 0$ and x/C, only the fourth term is active. At $t = x/C$, the first term is turned on. At $t = (d - x)/C$, the third term is turned on and u starts to decrease. At $t = (x + d)/C$, the second term is turned on and u becomes 0. At that time, wind forcing is balanced by the pressure gradient at that position. This results

$$\begin{aligned}
u &= Tt && 0 \le t < x/C \\
u &= Tx/C && x/C \le t < (d-x)/C \\
u &= Tx/C - T\{t - (d-x)/C\}/2 && (d-x)/C \le t < (x+d)/C \\
u &= 0 && (x+d)/C \le t
\end{aligned}$$

The friction coefficient r is, more or less, an empirical value and expected to be different from one fjord to the other. The value of the friction coefficient used here was chosen by comparing variances of the model transport and observation during the entire periods (45 days) when model is applied. The variance of model transport increases (decreases) as friction coefficient decreases (increases). We made several test run and then computed variances. Afterward, we selected the most matched friction coefficient with the variance of observation up to two significant digits, 4.0×10^{-5} sec^{-1}. The value of C is estimated to be 0.4 m/s.

Adding the constricted area as a sill at the seaward boundary is possible for the boundary value problem (Appendix). As shown in the Appendix, the boundary conditions proposed by FA are sufficient with the values of parameters chosen for the frequency range between 0.1 and 0.7 cpd.

3.2 Solution of initial value problem applied to Puget Sound

3.2.1 Comparison between observation and model

To compare observation and model results, cross-channel averaging was applied to the data. Band-pass filtering described before was applied prior to cross-channel averaging. Figure 3 shows the time series of transports averaged across the channel integrated from the surface to 30 m and integrated from 30 m to the bottom. To make the comparison easier, the latter is multiplied by –1. This figure shows that transport in the upper and lower layers, separated at 30 m, almost balances from about April 30, and it indicates the variation of the transport is very strongly baroclinic. The time series of salinity measured by RCM-4's shows that a relatively large salinity difference between 5 m and 19 m persists for about a month from April 29. When stratification is strong, propagation of events from the surface appears to be limited within the upper 30 m. It follows that, the application of a two-layer model with an interface depth of 30 m is reasonable

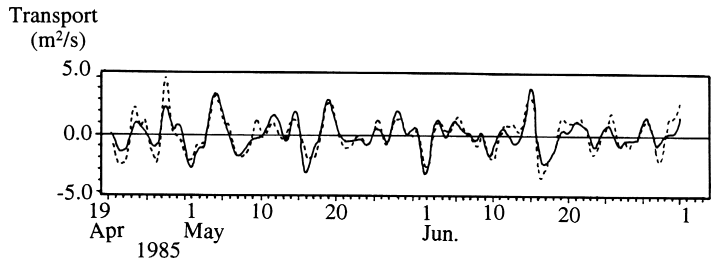

Fig. 3. The time series of the cross channel averaged transports between the surface and 30 m (solid line), and between 30 m and 200 m (dashed line). The latter time series is multiplied by –1.

for studying the dynamics for the latter part of the 1985 observation period. Therefore, in this subsection, the band-pass filtered cross-channel averaged values integrated from the surface to 30 m are compared with the results of the model. It is also noted that only the baroclinic mode is considered since the data show that the currents are strongly baroclinic with the upper and the lower layer separated at 30 m (Fig. 3).

The transport has been computed from Eq. (4) using Eq. (5). In these computations, d is 70 km and x is 31.5 km which is the approximate distance of the observation site from the Narrows. Figure 4(a) shows the time series of the cross channel averaged transport and the model transport. The model was started from April 1 which is 10 days before the beginning of the observation (Fig. 3) to avoid the effect of the initial condition. There are two peaks at about 0.16 and 0.37 cpd on the variance preserved spectra of both cross channel averaged transport and model result and coherence squared between them at these frequencies are over 0.8 (Fig. 4(b)). The difference between the observations and the model transport during the first several days is rather large. This is probably because stratification is too weak to apply the two-layer model during this period. The results of the model computations for the periods earlier than this show similar deviations.

Figure 5 shows the time series of the wind stress, which is proportional to the forcing, the acceleration of the measured transport averaged across the channel, and the acceleration of baroclinic transport computed by the model. As described before, there are events when acceleration decreases and changes sign while the wind continuously blows in the same direction. These phenomena are rather common and typical examples are from May 15 to May 17 and from June 14 to June 16, noted as α and β on the figure. Note that phase lag between forcing and acceleration can be seen clearly during the events beginning May 25. These results suggest that this model performs very well in reproducing the responses of currents in Puget Sound to wind forcing when stratification is strong enough to justify usage of the two-layer model. Some of the disagreements may be due to the lack of consideration of changes in stratification in the model. The result of EOF analysis applied to the axial currents shows that the EOF mode 1 is almost identical to this cross-channel averaged transport. These two time series are highly correlated (0.98), and this suggests that the cross-channel averaged transport does not contain components corresponding to EOF mode 2 or higher EOF modes. This implies that the computation of transports with the separation depth at 30 m filters out components such as bottom water intrusion (Bretschneider *et al*., 1985). Also, wind stress may not be uniform over the region.

3.2.2 Responses of acceleration and other terms

Figure 6 shows time series of the acceleration, the baroclinic pressure gradient, the forcing and the friction as described in Eq. (1). The forcing and the friction are almost, but not exactly,

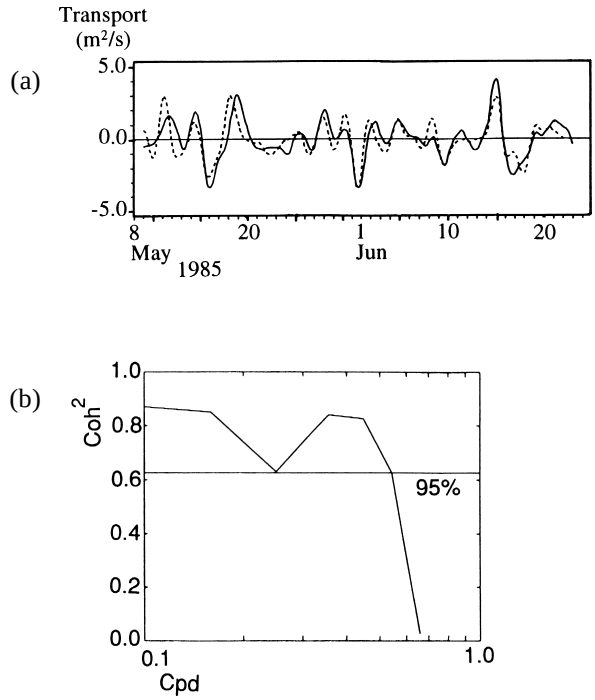

Fig. 4. (a) The time series of the cross channel averaged transport in the upper layer (solid line) and the baroclinic transport in the upper layer computed by the model (dashed line). (b) Cross coherence spectrum between cross channel averaged transport in the upper layer and the baroclinic transport computed by the model. 95% confidence limit is shown by horizontal solid line.

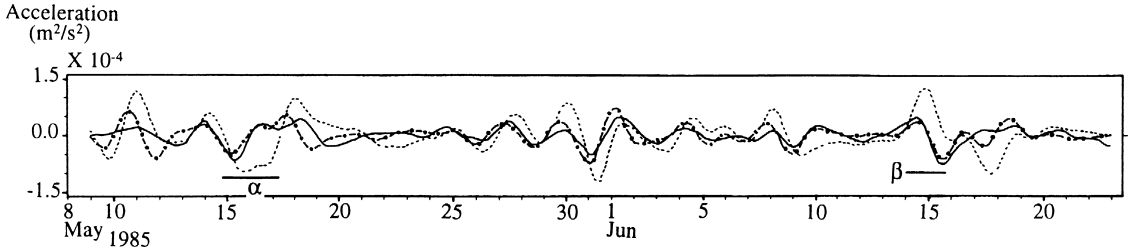

Fig. 5. The time series of the cross channel averaged acceleration integrated in the upper layer (—), model result (-·-) and the wind stress (- - -). The events noted as α and β are the cases when the observed acceleration shows considerable differences from the wind forcing.

out of phase. The negative acceleration prior to the turning of wind southward on May 15 (event α) is caused by friction which develops as the current increases. Since the change of the current is the result of the acceleration, a time lag between an increase of forcing and of friction is expected. With $C = 0.4$ m/s, the baroclinic pressure gradient starts changing about one day after the wind event. This time lag corresponds to the time necessary for the wave front to propagate from the head to the middle point. When the forcing period is relatively long, it appears that the phase lag between forcing and friction becomes small. If the duration of the event is longer than

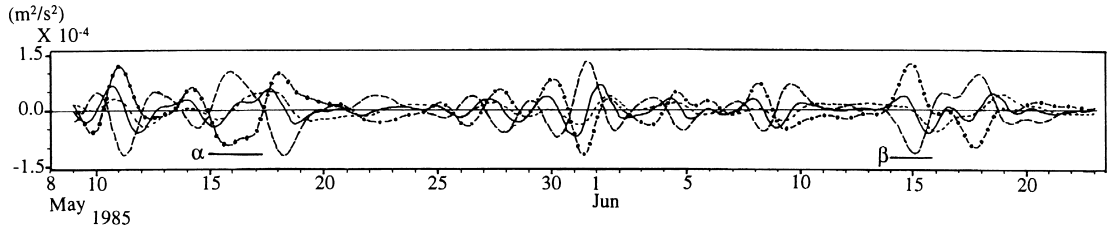

Fig. 6. The time series of acceleration ($\partial u/\partial t$, —), baroclinic pressure gradient ($C^2\partial\eta/\partial x$, - - -), forcing ($Tw$, -·-) and friction ($-Au$, – – –). The events noted as α and β are the same as in Fig. 5. The relation between these terms is $\frac{\partial u}{\partial t} = C^2 \frac{\partial \eta}{\partial x} + Tw - ru$.

about one day, changes of baroclinic pressure gradient due to that particular event start to take place. Here the duration of the event is defined by the time during which the wind blows in one direction. The event α shows this situation. Further discussion of the effects of forcing frequency on the transport is presented later.

When C = 0.7 m/s, the baroclinic pressure gradient is larger than for C = 0.4 m/s. The reason is that if C is larger, then less attenuation is expected due to the shorter transit time from the boundaries. The baroclinic pressure gradient, especially for the events of short duration, has more effect when compared with the case of C = 0.4 m/s. When the friction coefficient, r, is 10 times smaller than in the standard case, the baroclinic pressure gradient grows larger than in the standard case and the acceleration is strongly affected by this term.

3.2.3 Effects of forcing frequency

To understand the different responses for the different forcing frequencies, sinusoidal forcing with frequencies of 0.1, 0.2, 0.3, 0.5 and 0.7 cpd are applied. Figure 7 shows the initial response, immediately after the forcing is turned on, and the "steady" response when each term becomes periodic. Note that these initial responses can not be reproduced by the solution of the boundary value problem (i.e., Eq. (A4)). During the first half of the period of the forcing, it is seen that the acceleration first increases but then starts decreasing and eventually turns negative in all cases although the forcing, Tw, is still positive. With the forcing frequency of about 0.3 cpd or lower, this phenomena is not only the result of the friction but also the result of the baroclinic pressure gradient. When the forcing frequency is higher, the effect of the baroclinic pressure gradient is zero during this initial period because of the transit time. When forcing frequency is 0.1 cpd, the phase lag between forcing and friction is larger than the one when forcing frequency is 0.2 cpd. When forcing frequency is 0.2 cpd, the phase lag between forcing and friction becomes almost zero and these two terms almost balance each other. Thus acceleration almost follows the variation of baroclinic pressure gradient at this forcing frequency. As the forcing frequency increases, the phase lag between forcing and friction increases and the difference between them affects the variation of acceleration more. The amplitudes of the acceleration tend to increase as the forcing frequency increases because of smaller time scale, while the amplitude of the baroclinic pressure gradient tends to decrease. The amplitude of the velocity during initial period first increases slightly due to the effect of baroclinic pressure gradient but then decreases as the forcing frequency increases.

As described before, it takes about a day for the baroclinic pressure gradient to propagate from the boundaries to the middle of the channel if C = 0.4 m/s. Then the response of the

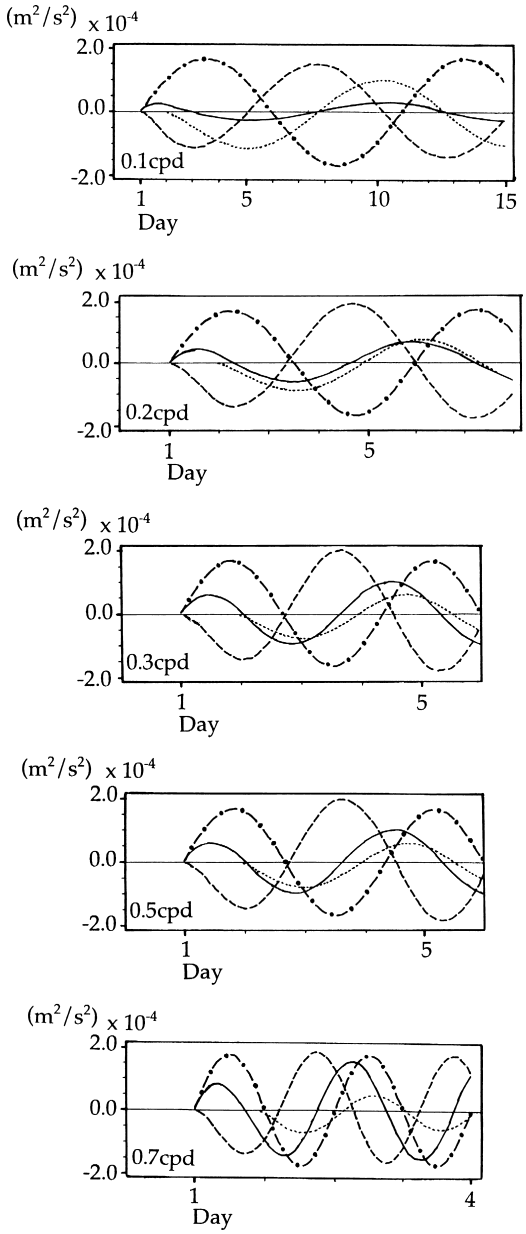

Fig. 7. The time series of acceleration (—), baroclinic pressure gradient (- - -), forcing (-·-) and friction (– – –) when forcing is sinusoidal. Forcing frequencies are noted on the figures.

acceleration can be described with the baroclinic pressure gradient set to zero for the first 22 hours at this location. In this case, with $Tw = T\sin\omega t$ where T is a constant, the solution is

$$u = \frac{T}{\sqrt{r^2 + \omega^2}}\left[\sin(\omega t - \theta) + e^{-rt}\sin\theta\right], \tag{7}$$

$$\frac{du}{dt} = \frac{T\omega}{\sqrt{r^2+\omega^2}}\cos(\omega t - \theta) - \frac{rT}{\sqrt{r^2+\omega^2}}e^{-rt}\sin\theta \tag{8}$$

where $\theta \equiv \sin^{-1}(\omega/\sqrt{r^2+\omega^2})$ and initial condition is $u = 0$ at $t = 0$.

These solutions show θ is the phase lag between forcing and friction. Note that friction is inversely proportional to the transport. When the forcing frequency is low, say an order of magnitude lower than the value of r (4×10^{-5} /s), which is about 0.06 cpd, the phase lag may be approximated as $\theta \cong \sin^{-1}(\omega/r) \cong \omega/r$. (However, it is noted here that 0.06 cpd is rather too low to ignore the effect of the baroclinic pressure gradient as shown in Fig. 7.) As the forcing frequency decreases, the phase lag and the amplitude of the acceleration decrease almost linearly while the amplitude of the velocity or transport asymptotically approaches a constant. When the forcing frequency is high, the above linear relation between the forcing frequency and the phase lag becomes invalid. As the forcing frequency increases, the phase lag asymptotically approaches a constant, $\pi/2$, while the amplitude of the velocity or transport decreases.

In general, these features can be seen in Fig. 7. As noted previously, Fig. 7 indicates phase lag between forcing and friction decreases as forcing frequency decreases from 0.7 cpd to 0.2 cpd. However, it also indicates that the amplitude of baroclinic pressure gradient increases as forcing frequency decreases and above simple analysis is no longer valid when forcing frequency is 0.1 cpd. Since the friction is the transport multiplied by a negative constant, $-r$, it appears that the variation of current precedes the variation of forcing when forcing frequency is 0.1 cpd (uppermost panel of Fig. 7; invert dash line (friction) and compare with dot-dash line (forcing)). This is caused by the effect of baroclinic pressure gradient which propagates from the boundary; i.e. the effect of the past event.

These results explain why the acceleration during the event α, the forcing period of which is about 3.5 days (0.14 cpd; note that the forcing period here is equivalent to the half cycle of forcing in Fig, 7), closely follows the baroclinic pressure gradient while the acceleration during event β, for which the forcing period is about 1.8 days (0.28 cpd), does not.

4. Conclusions

The solution for the baroclinic transport of a two-layer model as an initial/boundary value problem, originally solved for the surface layer thickness by Farmer (1976), was developed here. In this paper, only the baroclinic mode was considered since data show that currents were strongly baroclinic. Therefore, the following descriptions of the two-layer model can be applied to both upper and lower layers except signs are opposite. The baroclinic transport and acceleration computed from the model agreed with the cross channel averaged transport and the acceleration in the observed upper layer. The model reproduced the observed reduction of the acceleration and eventual reversal of the sign of the acceleration during wind events. The result of this model indicates that this phenomena is mainly caused by the friction. Further analysis, using a simplified equation and sinusoidal forcing, indicates that this phenomena is affected by the forcing frequency and the friction coefficient. The phase lag decreases almost linearly as forcing frequency decreases at low frequency range using the friction coefficient chosen for Puget Sound. As a result, when the forcing frequency is low (below 0.2 cpd), the baroclinic pressure gradient becomes more important in acceleration because the forcing and the friction terms almost balance each other while the amplitude of the baroclinic pressure gradient increases, and the transit times from the boundaries become smaller relative to the forcing period. As forcing frequency increases, the phase lag between the forcing and the friction increases and

the mismatch between them has a large effect on the acceleration while the amplitude of the baroclinic pressure gradient decreases and thus its effect on acceleration decreases.

Acknowledgements

The author thanks Dr. Cannon and other people for their comments to refine this paper.

Appendix

The model developed by Farmer (1976), referred as model 1, does not include the sill at the mouth and quantitative study of the effect of a sill at the seaward boundary is necessary. Adding the constricted area as a sill to the model is possible for the boundary value problem. The solution for the boundary value problem for the model I was obtained by Farmer for the sinusoidal forcing, $Tw = Te^{i\omega t}$ between $x = 0$ and $x = d$. From equation in the appendix of FA,

$$u = e^{i\omega t}\left[\left(\frac{1}{2}e^{-\gamma d} - 1\right)e^{-\gamma x} - \frac{1}{2}e^{-\gamma(d-x)} + 1\right]\frac{iT}{C^2\gamma^2} \quad \text{where} \quad \gamma = \frac{1}{C}\sqrt{i\omega r - \omega^2}. \tag{A1}$$

The modified model, referred as model II, uses different values for r, the friction coefficient and for C, the phase speed, either side of the mouth; that is, in the fjord, $0 \le x < d$ and beyond the mouth, $d \le x$. The basic idea is that if the cross sectional area decreases because of the sill, the velocity should increase to have the same amount of transport as shown by Geyer and Cannon (1982), and therefore, the friction should also increase. Figure A1 shows the configuration of model II.

Let $r = r_1$, $C = C_1$ for $0 \le x < d$ and $r = r_2$, $C = C_2$ for $d \le x$. Then, from Eqs. (1), (2) and equations of continuity,

$$\frac{\partial^2 u}{\partial t^2} = C_1^2\frac{\partial^2 u}{\partial x^2} + \frac{\partial}{\partial t}\left(Tw - r_1 u\right) \quad \text{for } 0 \le x < d \tag{A2}$$

$$\frac{\partial^2 u}{\partial t^2} = C_2^2\frac{\partial^2 u}{\partial x^2} - r_2\frac{\partial u}{\partial t} \quad \text{for } d \le x. \tag{A3}$$

Using the same boundary conditions, matching conditions and forcing as in the original model, the real part of the solution is

$$u = -\sqrt{F^2 + G^2}\,\sin\left(\omega t - \phi\right) \tag{A4}$$

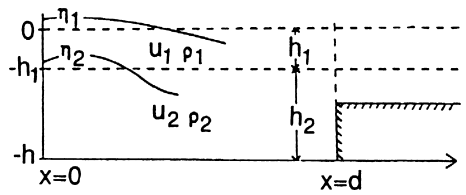

Fig. A1. The configuration of modified model.

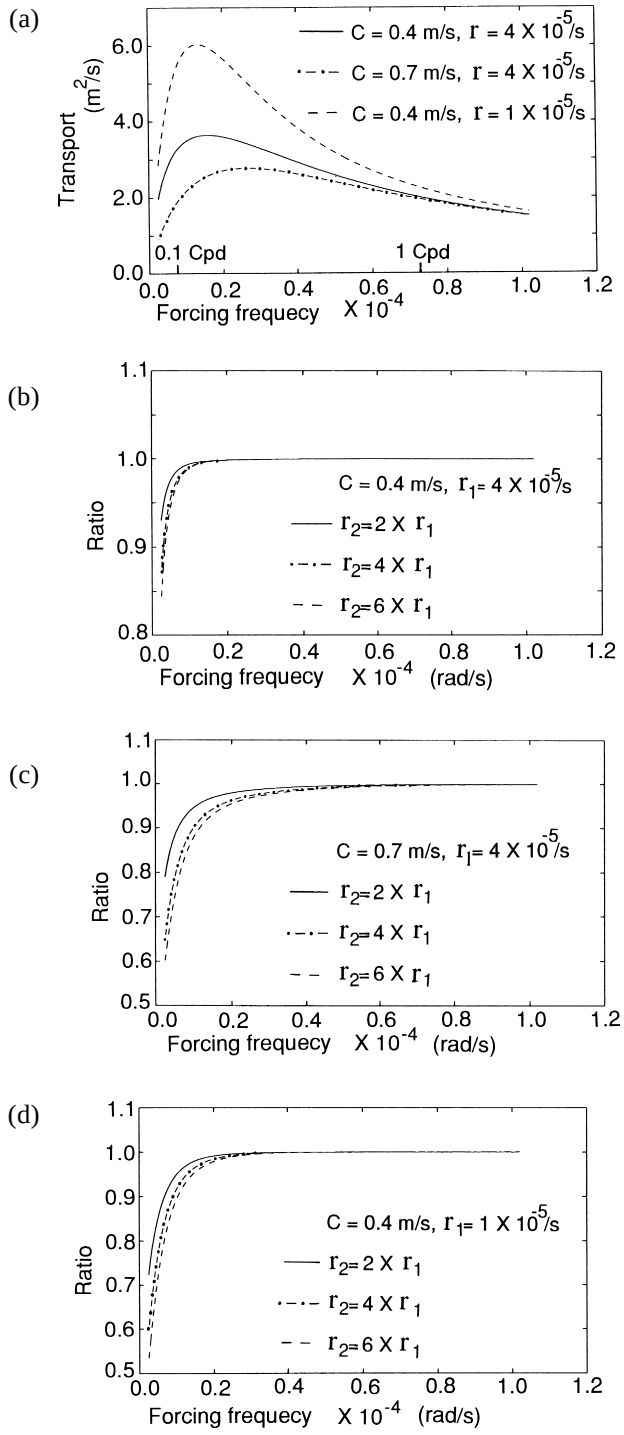

Fig. A2. (a) The baroclinic transport computed from the Farmer's model (model I) as a function of forcing frequency. (b)–(d) The ratio of the baroclinic transport of the modified model (model II) to the baroclinic transport of the Farmer's model (model I) as a function of forcing frequency. The values of the parameters are noted on the figures.

where F, G and ϕ are the functions of x, d, r_1, r_2, C_1, C_2, ω and T, but exact form is omitted here due to their excessive length (Matsuura, 1992). The detail of the method to obtain this solution is basically the same as FA. If $r_1 = r_2$ and $C_1 = C_2$, this solution reproduces the real part of the Farmer's solution shown in Eq. (A1).

Figure A2(a) shows the amplitude of the transport computed using model I, the real part of Eq. (A1), and Figs. A2(b), (c) and (d) show the amplitude ratio of the transports computed using model II to those computed using model I. The channel length, d, is 70 km and the x position, where ratios are computed, is x = 31.5 km. For the model I, the values of r and C are the same as r_1 and C_1 and these values are approximate for Puget Sound. Figure A2(a) indicates that the transport increases rapidly as a forcing frequency increases and after the maximum the transport decreases gradually. The frequency of the lowest mode of the internal seiche (for a channel with one open end) is 0.12 cpd. The damping is large enough to suppress internal seiche. This topic has been discussed by Farmer (1976) and with the values of parameters used here (c = 0.4 m/s and $r = 4 \times 10^{-5}$ /s), the length of the channel must be less than about 31.3 km to have oscillatory solution.

The amplitude ratio is close to unity at high frequencies of the sub-tidal range. As the forcing frequencies become lower, the amplitudes of the transports computed by model II become smaller than those computed by model I because the amplitude of the baroclinic pressure gradient increases as forcing frequency decreases. The ratio becomes smaller as r_1 decreases, r_2 increases, or C_1 (in this computation, C_2 has same value) increases. If r_1 decreases, the effect from the mouth is less attenuated while propagating from the mouth as a form of waves to the point x, and the same is true for larger C due to the shorter transit time. The results of these computation indicate that the boundary conditions proposed by FA are sufficient with the values of parameters chosen for the frequency range between 0.1 and 0.7 cpd.

References

Bretschneider, D. E., G. A. Cannon, J. R. Holbrook and D. J. Pashinski (1985): Variability of subtidal current structure in a fjord estuary: Puget Sound, Washington. *J. Geophys. Res.*, **90**, 11949–11958.

Buckley, J. R. and S. Pond (1976): Wind and the surface circulation of a fjord. *J. Fish. Res. Board. Can.*, **33**, 2265–2271.

Cannon, G. A. (1983): An overview of circulation in the Puget Sound estuarine system. *NOAA Tech. Memo.*, ERL PMEL-48, 30 pp.

Cannon, G. A. and N. P. Laird (1978): Variability of current and water properties from year-long observations in a fjord estuary. p. 515–535. In *Hydrodynamics of Estuaries and Fjord*, ed. by J. C. J. Nihoul, Elsevier, Amsterdam.

Farmer, D. M. (1976): The influence of wind on the surface layer of a stratified inlet: Part II. Analysis. *J. Phys. Oceanogr.*, **6**, 941–952.

Farmer, D. M. and T. R. Osborn (1976): The influence of wind on the surface layer of a stratified inlet: Part I. Observations. *J. Phys. Oceanogr.*, **6**, 931–941.

Geyer, W. R. and G. A. Cannon (1982): Sill processes related to deep water renewal in a fjord. *J. Geophys. Res.*, **87**, 7985–7996.

Gill, A. E. (1982): *Atmosphere-Ocean Dynamics*. Academic Press, London, 662 pp.

Hansen, D. V. and M. Rattray, Jr. (1965): Gravitational circulation in straits and estuaries. *J. Mar. Res.*, **23**, 104–122.

Matsuura, H. (1992): Wind effect on the sub-tidal current in Puget Sound. Ph.D. Dissertation, University of Washington, 178 pp.

Svendsen, H. and R. O. R. Y. Thompson (1978): Wind-driven circulation in a fjord. *J. Phys. Oceanogr.*, **8**, 703–712.

Tee, K. T. (1989): Subtidal salinity and velocity variations in the St. Lawrence estuary. *J. Geophys. Res.*, **94**, 8075–8090.